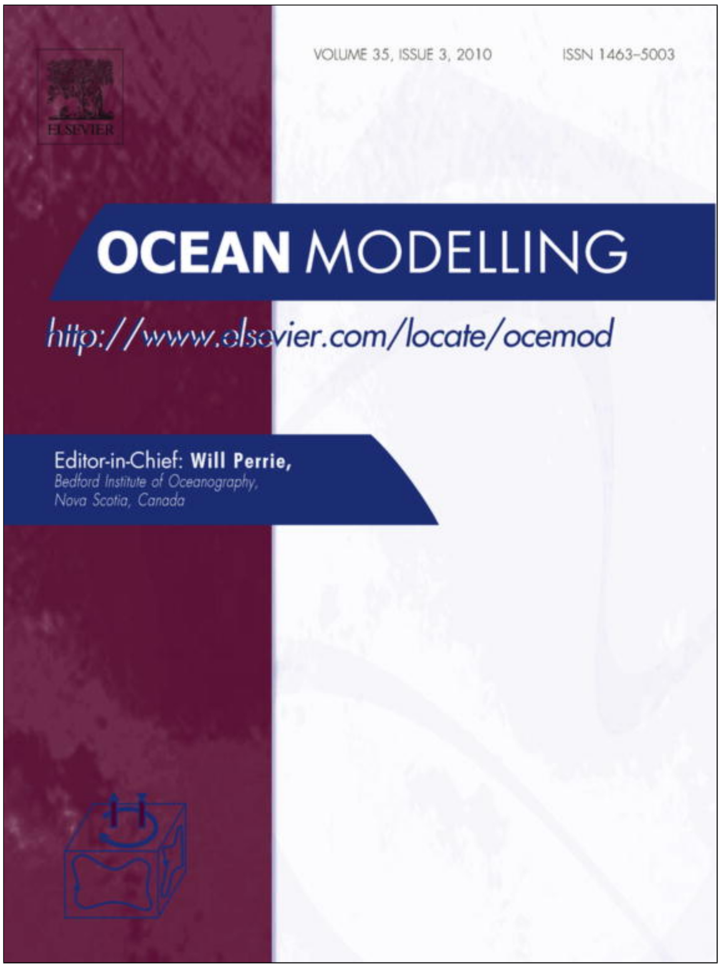
VOLUME 35, ISSUE 3, 2010
ISSN 1463-5003
ELSEVIER
OCEAN MODELLING
http://www.elsevier.com/locate/ocemod
Editor-in-Chief: Will Perrie,
Bedford Institute of Oceanography,
Nova Scotia, Canada

Ocean Modelling 35 (2010) 264–269

Contents lists available at ScienceDirect

Ocean Modelling

journal homepage: www.elsevier.com/locate/ocemod

Short communication

Comparison between a non-hydrostatic numerical model and analytic theory for the two-layer exchange flows

Mehmet Ilıcak [a,*], Laurence Armi [b]

[a] Atmospheric and Oceanic Sciences Program, Princeton University, Princeton, NJ 08540, USA
[b] Scripps Institution of Oceanography, La Jolla, CA 92093-0225, USA

ARTICLE INFO

Article history:
Received 20 January 2010
Received in revised form 5 May 2010
Accepted 10 May 2010
Available online 2 June 2010

Keywords:
Two-layer hydraulic control
Exchange flow

ABSTRACT

Recently, Armi and Riemenschneider (2008) improved the two-layer hydraulic theory and applied it to the co-located sill and contraction. The main goal in this study is to compare the new theory with a non-hydrostatic numerical model. To this end, the numerical model is employed for two different geometries. The first geometry is steep topography with co-located contraction and the second geometry is a much gentler slope so that the non-hydrostatic forces are reduced. It is found that the model captures the two control points, a topographic control at the crest and a virtual control on the dense reservoir side described by the theory. The flow is subcritical in between these control points. There is agreement between the modeled and analytical interface heights in the gentler topography.

1. Introduction

The flow between two basins with different densities is an important problem in geophysical fluid dynamics. Most of the marginal seas are connected to the ocean basins by straits containing shallow sills and/or lateral contractions e.g., the Strait of Gibraltar (Price and Baringer, 1994), the Bosphorus Strait (Gregg and Ozsoy, 2002), the Denmark Strait (Gordon et al., 2004), the Bab al Mandeb Strait (Peters et al., 2005). These two-layer exchange flows are important for intermediate and deep water formations which play a crucial role in the thermohaline circulation. These density driven flows are also important for exchange of water between an estuary and the open ocean. The seminal work on these is that of Stommel and Farmer (1953) who argued that, beyond a certain amount, mixing within the estuary increased neither the exchange nor the density of the surface layer. They called this limiting example "overmixing". Exchange flows are often called "lock-exchange flows" (Wood, 1970) based on how they are started in the laboratory or in the engineering application by withdrawing a barrier between the reservoirs. In fact the numerical computations pursued here were started in this way.

To understand the dynamics of exchange flows, an inviscid, steady two-layer theory was developed using an idealized channel with slowly varying geometry (Armi, 1986; Armi and Farmer, 1986; Lawrence, 1990). This two-layer hydraulic theory predicts the interface heights of the layers given the channel geometry, the densities of the layers and the flow rate ratio.

Increased computational power now allows high resolution non-hydrostatic models to simulate idealized and realistic cases of exchange flows (Winters and Seim, 2000; Ilıcak et al., 2008, 2009). Winters and Seim (2000) examine simulations of exchange flows through idealized contracting channels with flat topography and compare the results with the theory developed by Armi and Farmer (1986). Winters and Seim (2000) concluded that two-layer inviscid theory gives reasonable predictions of the layer interface heights. Ilıcak et al. (2009) used a laterally-averaged 2D non-hydrostatic model to conduct a set of numerical experiments of the lock-exchange problem in the presence of lateral and vertical contractions.

The analytical treatments for two-layer exchange flow through a contraction are given by Armi and Farmer (1986) and Lawrence (1990). However, in these studies the bottom topography is kept constant. Farmer and Armi (1986) modified the theory for the combination of a sill and contraction, however the sill and the contraction are not co-located. Recently, Armi and Riemenschneider (2008) improved the two-layer hydraulic theory and applied it to the co-located sill and contraction. The main aim in this study is to compare the numerical model results with this new theory. To this end, a 2D non-hydrostatic model is employed in a similar geometry to that required by Armi and Riemenschneider (2008). The modeled interface heights are compared with theoretical predictions as well as Froude numbers. It is found that the model captures the subcritical flow region between the virtual and topographic control. In addition, the modeled interface height is

* Corresponding author.
E-mail addresses: mehmet.ilicak@noaa.gov, milicak@rsmas.miami.edu (M. Ilıcak).

1463-5003/$ - see front matter © 2010 Elsevier Ltd. All rights reserved.
doi:10.1016/j.ocemod.2010.05.002

in agreement with the predicted interface heights given by the theory when the non-hydrostatic forces are reduced.

2. Theory

The non-dimensional continuity equation and the energy (Bernoulli) equation will be employed to describe the flow. For two-layers the flow is defined as critical when the composite Froude number, G, is equal to unity

$$G^2 = F_1^2 + F_2^2, \quad (1)$$

where F_1 and F_2 are layer Froude numbers defined as $F_i = u_i/\sqrt{g'y_i}$ (for $i = 1,2$), u_i is the flow speed, y_i is the layer thicknesses (Fig. 1) and $g' = g\Delta\rho/\rho_2$ is the reduced gravity ($\Delta\rho = \rho_2 - \rho_1$). The critical condition (Eq. (1)) is a straight line which separates subcritical ($G^2 < 1$) from supercritical flow ($G^2 > 1$) when plotted in the Froude number plane (Fig. 2).

The steady flow solutions are shown in the Froude number plane. Previous studies generally treat the contraction and sill separately. Therefore, two different Froude number planes were required for contractions and sills. The main reason behind this is that there is a fundamental physical difference between flow over a sill and flow through a contraction. The latter affects both layers in the exchange flow, however the sill only contacts the bottom layer (Farmer and Armi, 1986). A recent study, (Armi and Riemenschneider, 2008) extended the theory of Armi (1986) for non-rotating two-layer hydraulics to a geometry with co-located sill and contraction. A brief summary for the two-layer hydraulics will be given in this section. For further information about the analytical formulations, the reader is referred to Armi and Farmer (1986), Farmer and Armi (1986), Lawrence (1990) and Armi and Riemenschneider (2008). Theory of two-layer exchange flows through a geometric constraint is also reviewed by Pratt and Whitehead (2007).

The critical flow line intersects both topographic and virtual controls. Since the flow is assumed as steady-state, the continuity equation can be written as $q_i = u_i b y_i$ for each layer (b is the contraction width). Using the definition of Froude number and continuity equation, a non-dimensional condition can be described that governs the flow,

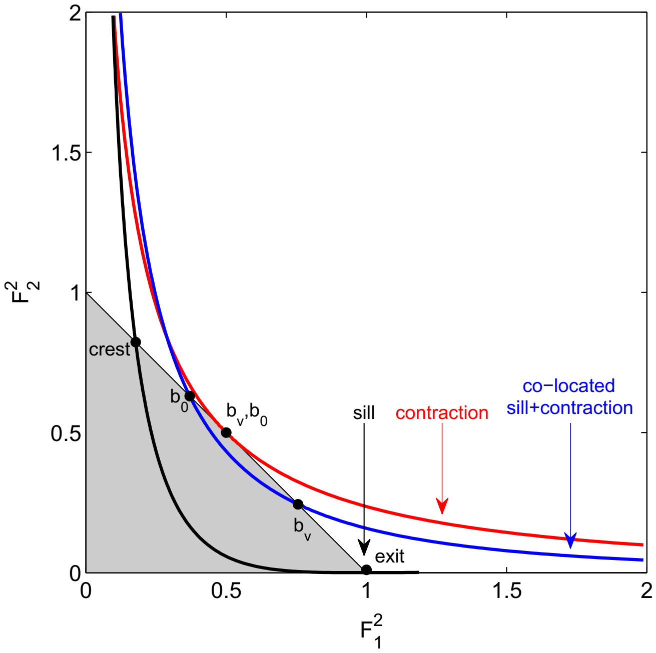

Fig. 2. Froude number plane for maximal exchange ($q_r = 1$) for different geometries. The subcritical region is shaded. In the sill case, the control points are at the crest and exit of the channel. In the contraction case, virtual and topographic controls (b_v,b_0) coincide at the narrow. In the co-located sill and contraction case, virtual control (b_v) is on the dense side of the topographic control (b_0).

$$\left[\frac{q_2'}{b'(1-h')^{3/2}}\right]^{-2/3} = q_r^{2/3}F_1^{-2/3} + F_2^{-2/3}, \quad (2)$$

where $q_r = q_1/q_2$ is the flow rate ratio, b' and q_2' are non-dimensional width and denser layer flow rate, respectively. Non-dimensional to-

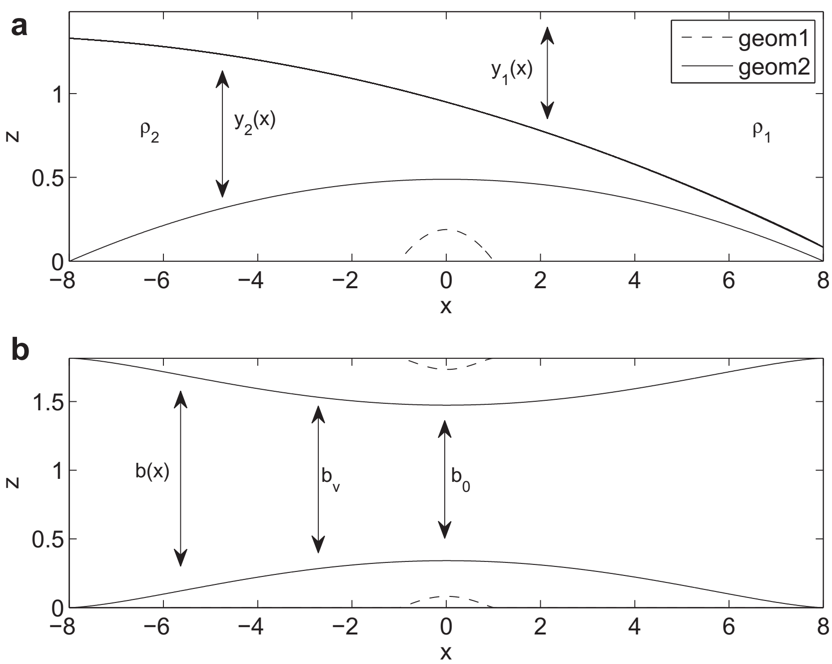

Fig. 1. Sketch of the geometries. (a) Side view of the *geom*1 and *geom*2 with top (y_1) and bottom (y_2) layers. (b) Plan view of the *geom*2. The control points for *geom*2 are shown by arrows and labelled b_0 for the primary control point at the top of the sill and b_v at the virtual control.

tal depth is also described as $(1-h')$. Eq. (2) defines the possible Froude number pairs for any given q_r and $q_2'/b'(1-h')^{3/2}$ for flows with co-varying contraction and sill. For flows through only a contraction, the non-dimensional height h' may be taken as zero, thus the contraction parameter is simply flow rate per unit width (q_2'/b'). However, for flows over a sill, the width remains constant and non-dimensional width, b', may be set to unity, thus the contraction parameter for flows over sill is $q_2'/(1-h')^{3/2}$.

Fig. 2 displays the three maximal exchange flows for sill, contraction and co-located sill + contraction cases. Note that, the actual flow rates, where the maximum exchange occurs, are different in these three cases. The solutions of the continuity equation for the three cases are not shown but they can be found in Armi and Farmer (1986), Farmer and Armi (1986) and Armi and Riemenschneider (2008). The subcritical region is also shaded. The maximal exchange flow through a contraction (red[1] curve) intersects with the critical flow line at one point where $F_1^2 = F_2^2 = 0.5$. This is the narrowest section of the contraction and the two-layers have the same thicknesses. On the other hand, the maximal exchange flow through a sill (black curve) intersects with the critical flow line at two control points; one is on the top of the sill and the other is at the exit of the channel (Fig. 2). The flow is subcritical ($G^2 < 1$) between these two control points. The maximum exchange flow through co-located sill and contraction (blue curve) has also two control points; one is the topographic control point at the crest/narrows (b_0 on blue curve in Fig. 2) and the other is the virtual control on the dense side of the topographic control b_v on blue curve in Fig. 2). In fact, there are always two control points for the maximum exchange and in the contraction case these two control points coincide at the narrowest point of the channel (b_v, b_0 on red curve in (2)). A striking feature in Fig. 2 is that the curve of the co-located sill + contraction case is similar to the curve of the pure contraction case. This means that when the contraction term is $b' = (1-h')^{3/2}$, the contraction controls the flow more than the sill for a combined sill and contraction geometry. In addition, the subcritical region in the co-located sill + contraction case is relatively smaller than the one in pure sill case.

3. Numerical model

In this study, a laterally-averaged 2D non-hydrostatic stream-function-vorticity model is employed. The non-dimensionalized model equations are

$$\frac{\partial \zeta}{\partial t} + \frac{1}{B}J(\psi,\zeta) + \zeta\frac{J(B,\psi)}{B^2} = -\frac{1}{Fr^2}\left(\frac{\partial \rho'}{\partial x}\right) + \frac{1}{Re}\nabla^2\zeta + \frac{1}{B}\frac{\partial}{\partial x}\left(\frac{B}{Re_t}\frac{\partial \zeta}{\partial x}\right) + \frac{1}{B}\frac{\partial}{\partial z}\left(\frac{B}{Re_t}\frac{\partial \zeta}{\partial z}\right), \tag{3}$$

$$\frac{\partial \rho'}{\partial t} + \frac{1}{B}J(\psi,\rho') = \frac{1}{RePr}\nabla^2\rho' + \frac{1}{B}\frac{\partial}{\partial x}\left(\frac{B}{Re_tPr_t}\frac{\partial \rho'}{\partial x}\right) + \frac{1}{B}\frac{\partial}{\partial z}\left(\frac{B}{Re_tPr_t}\frac{\partial \rho'}{\partial z}\right), \tag{4}$$

$$\nabla\cdot\left(\frac{1}{B}\nabla\psi\right) = \zeta, \tag{5}$$

where ζ is the vorticity, ψ is the stream function, ρ' is the density perturbation from the mean state, and B is the width of the domain. The Jacobian $J(a,b) = \frac{\partial a}{\partial x}\frac{\partial b}{\partial z} - \frac{\partial b}{\partial x}\frac{\partial a}{\partial z}$ is discretized using the Arakawa (1966) scheme to conserve both energy and enstrophy.

[1] For interpretation of colour in Figs. 5, 7 and 8, the reader is referred to the Web version of this article.

Model parameters are set as follows. Turbulent Prandtl number, Pr_t, is taken as 1 which corresponds to the case where eddy viscosity is equal to eddy diffusivity. The bulk Froude number and Reynolds number are taken as $Fr = 1$ and $Re = 10{,}000$, respectively. All the parameters above are carried over from Ilıcak et al. (2009). There are 2048 and 64 grid points in x and z directions, respectively. A Richardson number dependent Smagorinsky model is employed to compute the turbulent Reynolds number, Re_t,

$$Re_t = \left[(C_S\delta_{2D})^2|\overline{\mathscr{S}}|f(Ri)\right]^{-1}, \tag{6}$$

where $C_S = 0.17$ is the Smagorinsky constant and $\delta_{2D} = \sqrt{\Delta x \Delta z}$ is the filter scale as a function of model resolution. $\overline{\mathscr{S}} = \frac{\partial U}{\partial z} + \frac{\partial W}{\partial x}$ is the non-dimensional shear, where $U = -\frac{\partial \psi}{\partial z}$ and $W = \frac{\partial \psi}{\partial x}$. The Richardson number $Ri = F^{-2}N^2/(\frac{\partial U}{\partial z})^2$ is the ratio of the square of the non-dimensional buoyancy frequency $N^2 = -\frac{\partial \rho'}{\partial z}$ and vertical shear. $f(Ri)$ is a function used in 2D lock-exchange studies by Özgökmen et al. (2007),

$$f(Ri) = \begin{cases} 1 & \text{for } Ri < 0, \\ \sqrt{1-\frac{Ri}{Ri_c}} & \text{for } 0 \leqslant Ri \leqslant Ri_c, \\ 0 & \text{for } Ri > Ri_c, \end{cases} \tag{7}$$

where $Ri_c = 0.25$ is the critical Richardson number. More details about the numerical solution of this 2D model can be found in Ilıcak et al. (2008, 2009).

4. Results

Two different geometries are employed in this study. Non-dimensional vertical deformation (sill) of the domain is carried out as follows:

$$z(x) = z_{max} + (1 - z_{max})(1 - h') \quad \text{for } x_1 \leqslant x \leqslant x_2, \tag{8}$$

where $h' = (x/A_0)^2$. Eq. (8) is chosen since it is identical to the geometry in the two-layer theory. The contraction term, B, is computed using $B = (1-h')^{3/2}$ as shown in Fig. 1(b). In the first experiment, $A_0 = 1$, $z_{max} = 1.188$ and x_1 and x_2 is set to -1 and 1, respectively (black curve in Fig. 1(a)). This geometry is very similar to the *geom2* in Ilıcak et al. (2009). In the second experiment, we use a much gentler slope to minimize the affect non-hydrostatic terms. Therefore, $A_0 = 8$, $z_{max} = 1.488$ and x_1 and x_2 is set to -8 and 8, respectively (solid black curve in Fig. 1(a)).

The simulations are initialized as lock-exchange problems: denser fluid ($\rho' = 1$) fills the right side of the domain and lighter fluid ($\rho' = 0$) fills the left side. Lock-exchange in flat topography is a well-studied problem. The reader is referred to Cantero et al. (2007) and Ilıcak et al. (2009) for recent numerical simulations. The main features are as follows: once the initial interface start tilting, two gravity currents are generated and they propagate to the opposite directions. These gravity currents are symmetric since free-slip boundary conditions are applied for both bottom and top surfaces. The shear along the interface between the two gravity currents leads to so-called Kelvin–Helmholtz (KH) instabilities. The direction of advection of the instabilities is away from the control points (see Fig. 3(a) the movie in Fig. 4). This phenomena is also predicted by the two-layer hydraulic theory.

Next, we compare the numerical model results with inviscid two-layer theory by Armi and Riemenschneider (2008). To this end, the model is integrated in time with open boundary conditions untill $t = 190$ s. The quasi-steady-state is established after $t = 30$ s (Fig. 3). The Neumann type boundary condition is applied for the stream function at $x = -8$ and $x = 8$ (i.e. $\partial\psi/\partial x = 0$) and Orlanski type boundary conditions are applied for both vorticity and density perturbation fields (i.e. $\partial\Phi/\partial t + C_x\partial\Phi/\partial x = 0$ where $\Phi = \psi, \rho'$ and C_x is the phase speed). The density and velocity fields

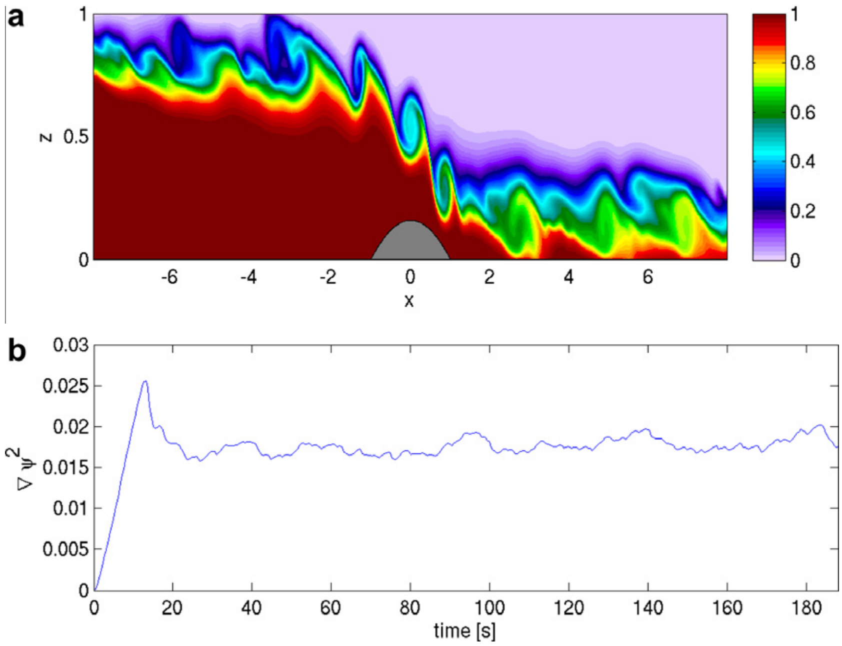

Fig. 3. (a) Snapshot of the density field for *geom*1 at time = 180 s. (b) Domain averaged kinetic energy vs time.

are time-averaged between $t = 50$ and $t = 190$ s (Figs. 4 and 5). The zero-isotach (i.e. $u = 0$) is chosen to separate the flow into two-layers and to form layer Froude numbers. The lower layer thickness, $y_2(x)$, is taken from the bottom to the height where $u = 0$, and the upper layer thickness $y_1(x)$ is then $z_{\max} - y_2(x)$. Layer velocities $u_1(x)$ and $u_2(x)$ are computed by vertically averaging local velocities within each layer. Since there is no net barotropic flow in the simulations, q_r is equal to unity.

The composite Froude number, G^2, and the bottom later Froude number, F_2^2, are plotted in Fig. 7(a) and Fig. 8(a) for *geom*1 and *geom*2, respectively. At the crest of the sill, both geometries display that $G^2 \approx 1$ as anticipated by the theory. To the right of the crest, the flow becomes supercritical (i.e. $G^2 > 1$). At the end of the sill for *geom*1, the composite Froude number suddenly drops to unity, and then increases till the end of the domain. We believe that this is due to a hydraulic jump at the end of the geometry. Fig. 6 displays the time-averaged density contours for *geom*1. Deformations of the density field at $x \approx -1.0$ and 1.5 cleary indicate a presence of a hydraulic jump. However, in the *geom*2, G^2 increases gradually since the co-located sill + contraction extend till the end of the domain.

At left side of the crest, the flow is subcritical ($G^{<}1$) in both simulations. The flow becomes critical at the virtual control point of each geometry (b_v in Fig. 7(a) and Fig. 8(a)). To the left of each virtual control point, the flow is supercritical again ($G^2 > 1$). The numerical simulations display that the virtual control is on the

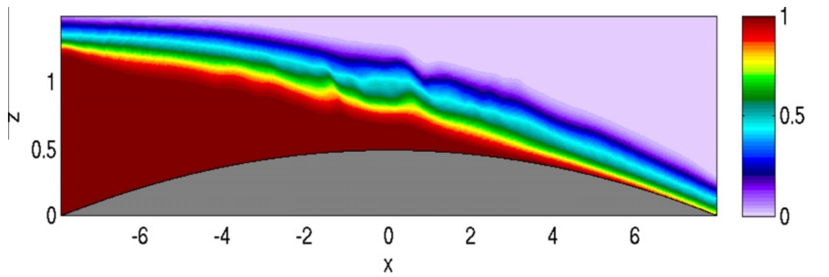

Fig. 4. Time-averaged density field for *geom*2. For the movie click the figure or go to <http://www.rsmas.miami.edu/personal/milicak/research/exchangeflow/exchangeflow.html>.

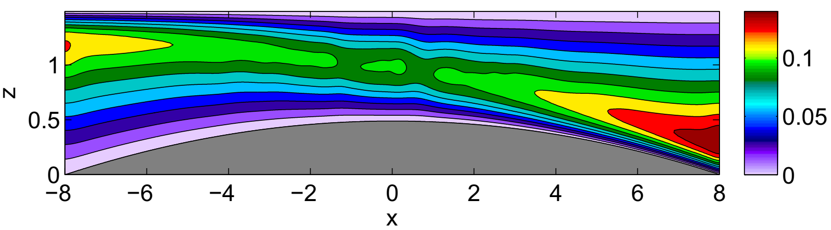

Fig. 5. Time-averaged stream function field for *geom*2.

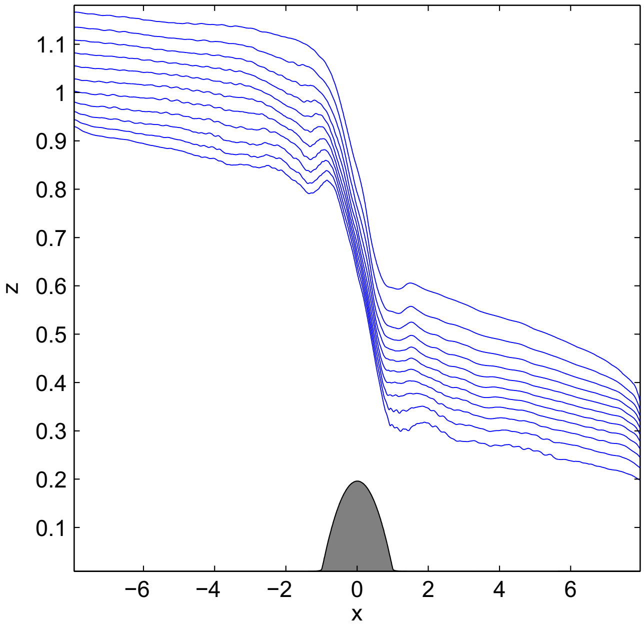

Fig. 6. Time-averaged density field for *geom*1. Contour interval is every 0.05 between $\rho' = 0.25$ and $\rho' = 0.55$.

dense fluid side of the crest as the analytical theory predicts. In Fig. 8(a), the computed Froude number curve is not smooth since the advection time scale of the instabilities is roughly 7 s and the 140 s time-averaged is not quite enough to remove all the noise.

Modeled and analytical interface heights are also plotted in Fig. 7(b) and Fig. 8(b) for *geom*1 and *geom*2, respectively. We use two different definitions for the modeled interface heights: one is the zero-isotach (black curve) and the other is the mid-isopycnal ($\Delta\rho' = 0.5$, blue curve). In the *geom*1, the modeled interface heights are below the theoretical interface at the left side of the crest and above the theoretical interface at the right side of the crest. The main reason behind this is presumably mixing in the model since the non-hydrostatic forces are dominant in the steeper topography. On the other hand, the interface heights in the *geom*2 display reasonable agreement with the predicted interface height (Fig. 8(b)). Gentler slope in the *geom*2 reduces the non-hydrostatic affects, thus mixing is limited.

Both simulations display some discrepancies from the analytic solutions especially with respect to the composite Froude numbers shown in Figs. 7 and 8. There seems to be another critical point at $x = -4$ in the *geom*1 (blue line Fig. 7(a)). The flow in the model goes through a hydraulic jump at $x \approx -1.5$ and slows down to the left of the sill due to friction. The flow behaves like a single layer flow for $x < -1$ since the dynamics is dominated by the upper layer. Friction reduces the Bernoulli energy and accelerates the single layer flow. It is expected that this "pseudo" critical point should be at the end of the domain, however probably reflection of the outgoing upper layer due to the open boundary conditions changes the location of the critical point. We believe that this is an artifact of the numerics but not the dynamics. The analytical theory predicts that the composite Froude number, G, is subcritical between the control points ($-1 < x < 1.5$), critical at the control points, subcritical to the left of the hydraulic jump ($x < -1$) and critical again at the exit of the domain ($x = -8$) since the channel expands at that point. In a perfect model, the open boundary is analogous to the physical situation that the channel expands at the end of the domain. Hence, the flow should be critical at $x = -8$ and subcritical to the right. In the model, this "pseudo" critical point appears to be shifted to the right because of our approximation to compute the G as a 2-layer system when in fact the stratification spreads out signifcantly in depth as shown in Fig. 6.

Another deficiency of the model is the sawtooth shape of the composite Froude numbers. Longer time-averaged helped to improve the plot of the G. However, there is mixing in the model and the interface is diffuse (Fig. 6), thus it is hard to define the layer location every grid points in x-direction.

5. Summary

The analytical theory predicts different interface heights for two-layer exchange flows through a sill, contraction and co-located sill and contraction (Fig. 2). Ilıcak et al. (2009) compared their model results for the sill + contraction case with contraction-only theory, however this was incorrect. The main goal in this study is to compare the model results to the theory developed by Armi and Riemenschneider (2008) for the co-located sill and contraction

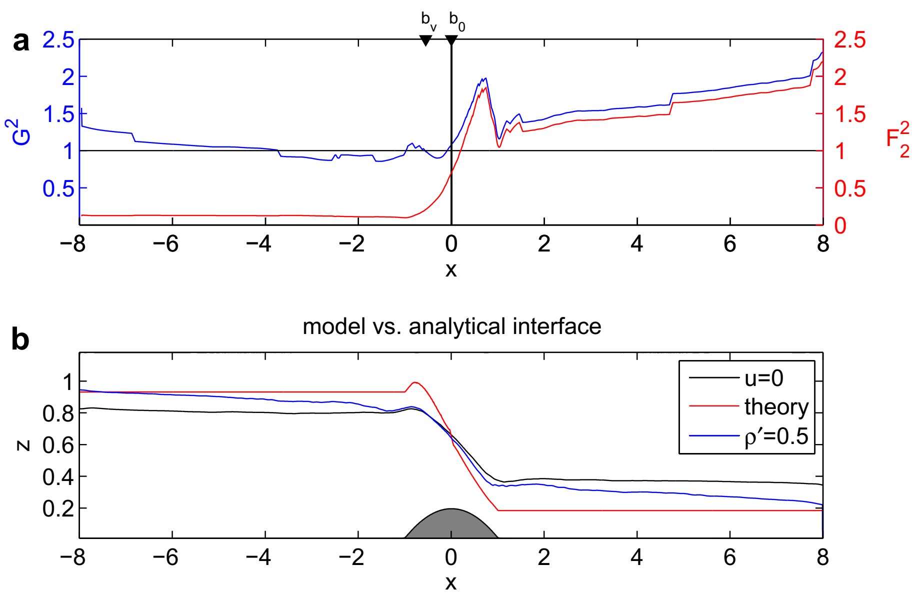

Fig. 7. (a) G^2 and F_2^2 for *geom*1, location of the virtual control is shown with an arrow. (b) Analytical and modeled interface heights for *geom*1.

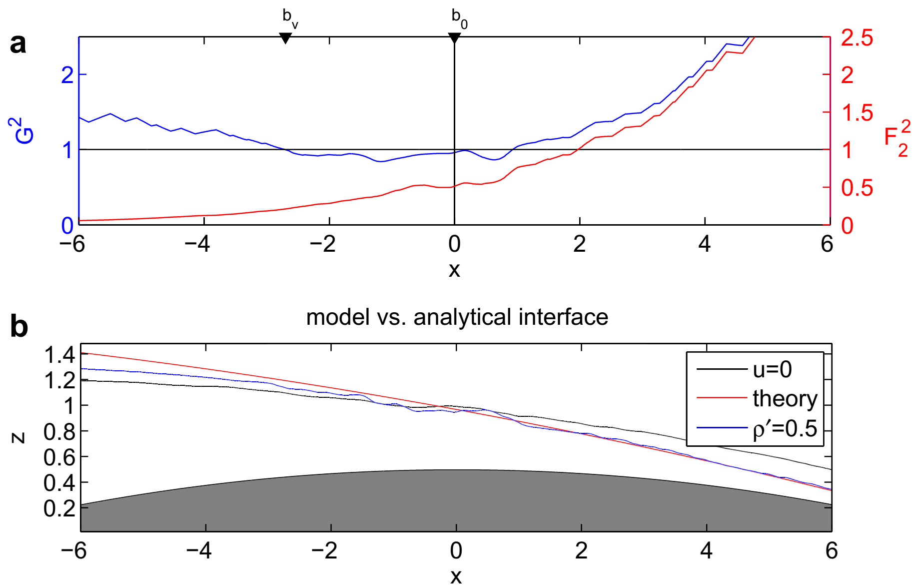

Fig. 8. (a) G^2 and F_2^2 for *geom*2, location of the virtual control is shown with an arrow. (b) Analytical and modeled interface heights for *geom*2.

case. We employ the same non-hydrostatic model used in Ilıcak et al. (2009) for two different geometries. The model result displays a topographic control at the crest and a virtual control on the dense reservoir side of the topographic control. The flow is subcritical in between these control points. There is a discrepancy between the modeled and analytical interface heights due to the mixing in the model in the steeper topography. We performed an additional experiment with the sill and contraction extending to the end of the domain. The main reason to use the second geometry is that the gentle slope reduces the non-hydrostatic affects. In the *geom*2, the distance between virtual and topographic control is increased. This time, the modeled interface height is similar to the predicted one of the analytical theory.

Acknowledgments

We thank the reviewers for their careful and constructive reviews. Ilıcak thanks to Tamay M. Özgökmen for his support. Armi thanks the Office of Naval Research, the University of California and Lucky Larry's Auto Repair for sustained financial support of his interest in stratified flows.

Appendix A. Supplementary data

Supplementary data associated with this article can be found, in the online version, at doi:10.1016/j.ocemod.2010.05.002.

References

Arakawa, A., 1966. Computational design for long-term numerical integration of the equations of fluid motion: two dimensional incompressible flow – Part I. Journal of Computational Physics 1, 119–143.
Armi, L., 1986. The hydraulics of two flowing layers with different densities. Journal of Fluid Mechanics 163, 27–58.
Armi, L., Farmer, D.M., 1986. Maximal two-layer exchange through a contraction with barotropic net flow. Journal of Fluid Mechanics 164, 27–51.
Armi, L., Riemenschneider, U., 2008. Two-layer hydraulics for a co-located crest and narrows. Journal of Fluid Mechanics 615 (November), 169–184.
Cantero, M.I., Lee, J.R., Balachandar, S., Garcia, M.H., 2007. On the front velocity of gravity currents. Journal of Fluid Mechanics 586 (August), 1–39.
Farmer, D.M., Armi, L., 1986. Maximal two-layer exchange over a sill and through the combination of a sill and contraction with barotropic flow. Journal of Fluid Mechanics 164, 53–76.
Gordon, A.L., Zambianchi, E., Orsi, A., Visbeck, M., Giulivi, C.F., Whitworth, T., Spezie, G., 2004. Energetics plumes over the western ross sea continental slope. Geophysical Research Letters 31 (21). Article No. L21302.
Gregg, M.C., Ozsoy, E., 2002. Flow, water mass changes, and hydraulics in the Bosphorus. Journal of Geophysical Research – Oceans 107 (C3), 3016. Article No. 3016.
Ilıcak, M., Özgökmen, T.M., Peters, H., Baumert, H.Z., Iskandarini, M., 2008. Very large eddy simulation of the Red Sea overflow. Ocean Modelling 20, 183–206.
Ilıcak, M., Özgökmen, T.M., Özsoy, E., Fischer, P.F., 2009. Non-hydrostatic modeling of exchange flows across complex geometries. Ocean Modelling 29, 159–175.
Lawrence, G.A., 1990. On the hydraulics of Boussinesq and non-Boussinesq two-layer flows. Journal of Fluid Mechanics 215 (June), 457–480.
Özgökmen, T.M., Iliescu, T., Fischer, P.F., Srinivasan, A., Duan, J., 2007. Large eddy simulation of stratified mixing in two-dimensional dam-break problem in a rectangular enclosed domain. Ocean Modelling 16, 106–140.
Peters, H., Johns, W.E., Bower, A.S., Fratantoni, D.M., 2005. Mixing and entrainment in the Red Sea outflow plume – Part I: Plume structure. Journal of Physical Oceanography 35, 569–583.
Pratt, L.J., Whitehead, J.A., 2007. Rotating Hydraulics: Nonlinear Topographic Effects in the Ocean and Atmosphere. Springer, New York, USA.
Price, J.F., Baringer, M.O., 1994. Outflows and deep water production by marginal seas. Progress in Oceanography 33, 161–200.
Stommel, H., Farmer, H.G., 1953. Control of salinity in an estuary by a transition. Journal of Marine Research 12, 13–20.
Winters, K.B., Seim, H.E., 2000. The role of dissipation and mixing in exchange flow through a contracting channel. Journal of Fluid Mechanics 407 (March), 265–290.
Wood, I.R., 1970. A lock exchange flow. Journal of Fluid Mechanics 42, 671–687.